Enhancement of exchange bias in ferromagnetic/antiferromagnetic core-shell nanoparticles through ferromagnetic domain wall formation

Rui Wu (吴锐),[1,3,4,*] Shilei Ding (丁石磊),[1,3] Youfang Lai (赖有方),[1,3] Guang Tian (田广),[1,3] and Jinbo Yang (杨金波)[1,2,3,*]

[1]*State Key Laboratory for Mesoscopic Physics, School of Physics, Peking University, Beijing 100871, People's Republic of China*

[2]*Collaborative Innovation Center of Quantum Matter, Beijing 100871, People's Republic of China*

[3]*Beijing Key Laboratory for Magnetoelectric Materials and Devices, Beijing 100871, People's Republic of China*

[4]*Department of Materials Science and Metallurgy, University of Cambridge, Cambridge, CB3 0FS, United Kingdom*

(Received 7 September 2017; revised manuscript received 6 January 2018; published 25 January 2018)

The spin configuration in the ferromagnetic part during the magnetization reversal plays a crucial role in the exchange bias effect. Through Monte Carlo simulation, the exchange bias effect in ferromagnetic-antiferromagnetic core-shell nanoparticles is investigated. Magnetization reversals in the ferromagnetic core were controlled between the coherent rotation and the domain wall motion by modulating the ferromagnetic domain wall width with parameters of uniaxial anisotropy constant and exchange coupling strength. An anomalous monotonic dependence of exchange bias on the uniaxial anisotropy constant is found in systems with small exchange coupling, showing an obvious violation of classic Meiklejohn-Bean model, while domain walls are found to form close to the interface and propagate in the ferromagnetic core with larger uniaxial anisotropy in both branches of the hysteresis. The asymmetric magnetization reversal with the formation of a spherical domain wall dramatically reduces the coercive field in the ascending branch, leading to the enhancement of the exchange bias. The results provide another degree of freedom to optimize the magnetic properties of magnetic nanoparticles for applications.

DOI: 10.1103/PhysRevB.97.024428

I. INTRODUCTION

Exchange bias has been found in magnetic materials containing exchange-coupled interfaces between two different magnetic phases. Being of great interest both for the applications in spintronic devices and fundamental physics of condensed matter physics, exchange bias has been extensively studied since it was discovered more than half a century ago [1]. Exchange bias has been found in a wide range of materials including low-dimensional composites with ferri-/ferromagnet (FM)/antiferromagnet (AFM) combinations [2–4], single-phase bulk materials with spin glass (SG), or super spin glass (SSG) [5–7]. Recently, a giant exchange bias effect has also been reported in magnetic single phases with intersublattice interactions [8–10]. Typical systems such as FM/AFM bilayers and FM/AFM core-shell nanoparticles usually serve as prototype models for the study of exchange bias, due to the well-defined FM and AFM parts as well as the interfaces.

Magnetic nanoparticles are of increasing appeal and have found numerous applications in engineering (magnetic recording media or magnetic seals) and biomedical applications (magnetic resonance imaging, drug delivery, or thermotherapy) [11]. With the first exchange bias reported in Co/CoO core-shell nanoparticles, in recent years, the study of exchange bias in nanoparticles and nanostructures has gained renewed interest since it has been shown that control of the core/shell interactions or of the exchange coupling between the particle surface and the embedding matrix can increase the superparamagnetic limit for their use as magnetic recording media [12]. Advances in techniques for synthesis of nanomaterials [13–15] allow the magnetic properties in both the core and the shell to be continuously controlled with morphology [16–19] and composition [20–23] tailoring. A number of factors have shown, in both experimental studies and Monte Carlo (MC) simulations, strong effects in the observed exchange bias or magnetic properties in the core-shell structures, including the core/shell thicknesses [24–27], particle shape/morphology [28,29], cooling field [30,31], dipolar interactions [32,33] /interparticle exchange interactions [11], and interface lattice/magnetic mismatch/disorder [34,35].

In the Meiklejohn-Bean (M-B) model, by assuming a collinear magnetization reversal in both FM and uncompensated AFM parts, the exchange bias field was predicted to be

$$h_E = \frac{\sigma_{\mathrm{ex}}}{t_{\mathrm{FM}} M_{\mathrm{FM}}}, \tag{1}$$

where σ_{ex}, t_{FM}, and M_{FM} stand for the interfacial exchange coupling energy, the FM thickness, and the FM magnetization, respectively. Thus an inversely linear dependence on the thickness of FM layer [36,37] and no dependence on intrinsic properties of FM part, including the magnetic anisotropy and the exchange coupling strength were indicated in the model. Since the M-B model works very well in many systems, the effect of inner magnetic structure in the FM part has been overlooked to some extent for quite a long time, while the most effort has been devoted to the magnetic structures in AFM parts and interfaces. However, recent experimental and theoretical

*Corresponding author: jbyang@pku.edu.cn; rw556@cam.ac.uk

results indicate that this rule can be violated, while a partial domain wall parallel to FM-AFM interface forms in FM layer during the magnetization reversal process [38,39]. Although nonuniform magnetization configurations have been reported in magnetic nanoparticles *via* small-angle neutron scattering [40,41] magnetic force microscopy [42], magnetic electron holography [43], and MC simulations [44–47], its effect on the exchange bias of FM-AFM core-shell structures and how it can be controlled remain unknown.

In this paper, it is shown, through MC simulations based on a simple model of single core/shell nanoparticle, how the formation of a spherical domain wall in the FM core is related to exchange bias in this system. The spherical domain wall is induced or suppressed in the FM core by tuning the domain wall width by varying the anisotropy constant and the exchange coupling strength. This result is confirmed by inspection of magnetic configurations and curls of magnetic configurations in the core along the hysteresis loops. It is further demonstrated that there is a formation of a spherical domain wall in the core, while magnetization reversal significantly reduces the coercive field in the ascending branch, and consequently enhances the exchange bias field.

II. MODEL

The considered nanoparticles have a spherical shape with a total radius of $R = 12a$, respectively, with a being the unit cell size. All the particles are made of an FM core surrounded by an AF shell of a constant thickness $R_{\mathrm{Sh}} = 3a$ with magnetic properties different from the core as well as from the spins at the interface between core and shell spins. Taking $a = 0.3$ nm, such a particle corresponds to typical real dimensions $R \approx 4$ nm with a fixed shell thickness of $R_{\mathrm{Sh}} \approx 1$ nm and contains 5575 spins, with 3071 spins in the FM core and 2504 spins in the AFM shell. The interface is defined to be the atoms in the AFM shell, which have direct exchange coupling with the FM core and contains 918 spins. The anisotropic Heisenberg spin model is adopted in the calculations with a Hamiltonian given by

$$\begin{aligned} H/k_B = &-J_{\mathrm{FM}} \sum_{\langle i,j\in \mathrm{FM}\rangle} \vec{S}_i \cdot \vec{S}_j - J_{\mathrm{AFM}} \sum_{\langle i,j\in \mathrm{AFM}\rangle} \vec{S}_i \cdot \vec{S}_j - J_{\mathrm{INT}} \\ &\times \sum_{\langle i\in \mathrm{FM},\, j\in \mathrm{AFM}\rangle} \vec{S}_i \cdot \vec{S}_j - K_{\mathrm{FM}} \sum_{\langle i\in \mathrm{FM}\rangle} \vec{S}_{iz}^2 - K_{\mathrm{AFM}} \\ &\times \sum_{\langle i\in \mathrm{AFM}\rangle} \vec{S}_{iz}^2 - \sum_{i=1}^{N} \vec{h} \cdot \vec{S}_i, \end{aligned} \tag{2}$$

where $\vec{S}_i$ are classical Heisenberg spins of unit magnitude placed at the nodes of a simple cubic lattice. The first row gives the exchange energy between spins located in FM core, AFM shell, and FM-AFM interface with exchange coupling constants denoted by J_{FM}, J_{AFM}, and J_{INT}, respectively. The second row gives the local anisotropic energy for each spin in FM core and AFM shell with the anisotropy constant represented by K_{FM} and K_{AFM}, respectively. The local anisotropy axes are set to be the z direction for all spins to impart a uniaxial anisotropy to the simulated systems. The last term describes the Zeeman coupling to an external field H applied along the easy-axis direction, which in reduced units reads $\vec{h} = \mu\vec{H}/k_B$ (with μ the magnetic moment of the spin) and will be denoted in temperature units [48].

To calculate the magnetic properties, the MC method with a standard Metropolis algorithm is employed [49]. As for the spin updates, an attempt to change the spin at a randomly picked site i from $\vec{S}_i$ to $\vec{S}_i'$ is made in a Monte Carlo trial step with the acceptance rate given by

$$P(\vec{S}_i \to \vec{S}_i') = \min[1, \exp(-\Delta E/k_B T)], \tag{3}$$

where ΔE denotes the change in free energy of the system if $\vec{S}_i'$ is accepted. To get an optimum efficiency for the Heisenberg system with finite uniaxial anisotropies, a combination of three kinds of trial steps, a uniform movement, a small movement, and a reflection, with a ratio of 3:1:1, is adopted [50]. In the uniform movement, the direction of $\vec{S}_i'$ is selected by random sampling on a sphere with Marsaglia method [51]. In the small movement, the direction of $\vec{S}_i'$ is selected by random sampling in a cone centered about $\vec{S}_i$. A reflection movement, where the direction of $\vec{S}_i'$ is selected to be $-\vec{S}_i$, is included to simulate nucleation processes even more efficiently in the limit of very large anisotropy.

An MC step (MCS) is finished while every spin in the whole system has undergone a trial step for once. To get the equilibrium state, at each field (or temperature) point, 10 000 MCSs are performed with 9800 MCSs for configuration relaxation and the remaining 200 MCSs for averaging the quantities, which is enough to minimize the fluctuation in the data, especially at low temperature. To get more detailed magnetization reversals around the coercive field, smaller field steps are used for the spin configuration calculation with keeping the total MCSs.

III. RESULTS AND DISCUSSION

A. The K_{FM} dependence of exchange bias

Systems with different ferromagnetic anisotropy constants, K_{FM}, are field cooled (FC) from a high-temperature (far above Néel temperature of AFM shell, T_N) disordered phase in a constant step down to the measuring temperature $T = 0.1$ K in the presence of a cooling field $h_{\mathrm{FC}} = 0.4J_0$ applied along the easy-axis direction, with $J_0 = 10$ K as a reference parameter. All the other parameters, the exchange coupling in FM core $J_{\mathrm{FM}} = J_0$, exchange coupling at the FM-AFM interface $J_{\mathrm{INT}} = -0.5J_0$, exchange coupling in AFM shell $J_{\mathrm{AFM}} = -0.5J_0$, and the anisotropy constant in the AFM shell $K_{\mathrm{AFM}} = J_0$, were kept the same within all systems, which was targeted to give a larger Curie temperature T_C of FM core than T_N and a relatively large anisotropy of AFM part due to the ultrathin thickness of the AFM shell [28]. The K_{FM}/J_0 is varied from 0 to 0.1, which is in the reasonable range for real ferromagnetic systems [52]. The temperature dependence of the normalized magnetizations M/M_S (with M_S being the total number of spins in the nanoparticle) in the core, the shell, and the interface in a system with $K_{\mathrm{FM}}/J_0 = 0.1$ is given in Fig. 1(a), where a paramagnetic to ferromagnetic transition is observed when temperature decreases across the Curie temperature ($T_{\mathrm{C}} \approx 15$ K) of the FM core and a paramagnetic to antiferromagnetic transition is observed when the temperature decreases across

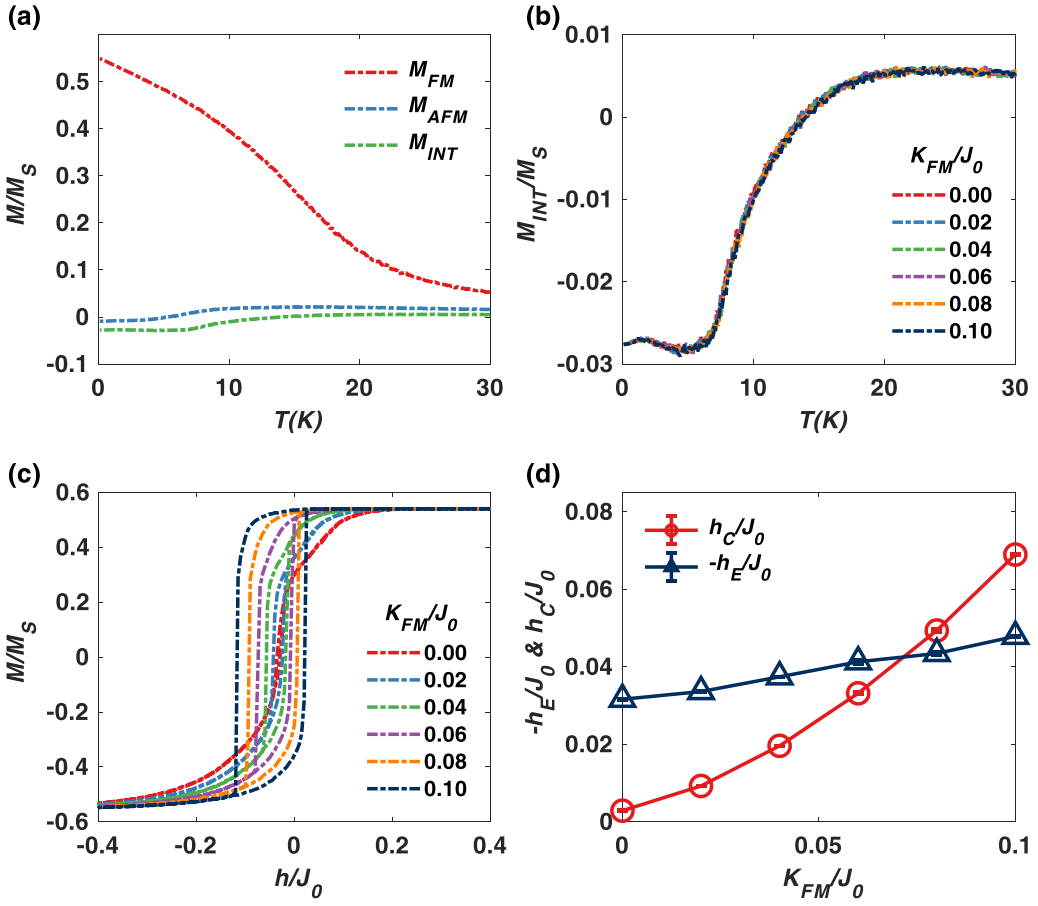

FIG. 1. (a) The FC M-T curves of different parts of the core-shell structure with $K_{\mathrm{FM}}/J_0 = 0.1$. (b) The FC M-T curves of interfacial spins, (c) hysteresis loops after FC, and (d) extracted h_E and h_C obtained in core-shell structures with $0 \leqslant K_{\mathrm{FM}}/J_0 \leqslant 0.1$. All the data in (d) are averaged with three independent calculations with error bars coming from the calculated standard deviations.

the Néel temperature ($T_N \approx 6.5\,\mathrm{K}$) of the AFM shell. Due to the antiferromagnetic exchange coupling at the interface between the FM core and the AFM shell, the uncompensated interfacial spins give a negative net magnetization. From Fig. 1(b), the interfacial net magnetization M_{INT} remains nearly invariant with increasing K_{FM} at all temperatures, indicating that the spin configuration in the FM core is dominated by the exchange coupling J_{FM} and the cooling field h_{FC}.

After the FC, hysteresis loop calculations are undertaken for each system with different K_{FM} using the starting configuration obtained with the FC process and by cycling the magnetic field from $h = 0.4J_0$ to $h = -0.4J_0$ in steps $h = -0.005J_0$. Integration of the magnetization is carried out over the whole system. As shown in FIG. 1(c), the hysteresis loops change significantly with the increasing uniaxial anisotropy constant of the FM core. As expected, a larger K_{FM} unambiguously gives a larger coercivity in the hysteresis loop where nearly zero coercive fields were obtained with $K_{\mathrm{FM}} = 0$ with the hard-axis switching characteristics presented, showing a progressive approach to both positive and negative saturation, due to the spin-flop coupling between FM spins and those compensated AFM spins at the interface [53–55]. As the K_{FM} increases, the induced anisotropy perpendicular to z axis is overwhelmed by the uniaxial anisotropy of the FM core itself, showing a sharper magnetization switching in both sides and a significantly enhanced coercivity. However, as shown in Fig. 1(d), it is found that the dependence of the coercivity h_C [defined as $h_C = (h_{\mathrm{CR}} - h_{\mathrm{CL}})/2$, where h_{CR} and h_{CL} are the left coercive field and right coercive field, respectively] on the K_{FM} is not linear. Moreover, the exchange bias field h_E [defined as $h_E = (h_{\mathrm{CR}} + h_{\mathrm{CL}})/2$] also shows a monotonic increase with increasing K_{FM}, which violates the result predicted by the M-B model where the exchange bias field only depends on the interfacial exchange coupling energy $\sigma_{\mathrm{ex}} \sim J_{\mathrm{INT}} M_{\mathrm{INT}}$ and the total magnetization of the FM part $t_{\mathrm{FM}} M_{\mathrm{FM}}$. Since both J_{INT} and t_{FM} are invariant with K_{FM}, to reveal the underlying origin of this effect, constrained MC calculations are undertaken, in which the AFM spins are fixed in the hysteresis loop calculations after the same FC process with the nonconstrained MC calculations. Thus the effect of the FM core behavior on the exchange bias can be studied separately.

As shown in Fig. 2, the hysteresis loops calculated with the constrained MC show similar K_{FM} dependence with those obtained with nonconstrained MC method especially when the K_{FM} is small, where the hysteresis also shows a hard-axis-like magnetization with the switching coming from the spin-flop coupling. However, with higher K_{FM}, the hysteresis shows higher asymmetry with sharper magnetization switching in the descending branch than the one obtained with nonconstrained MC; this effect is ascribed to the rigidness of the interfacial

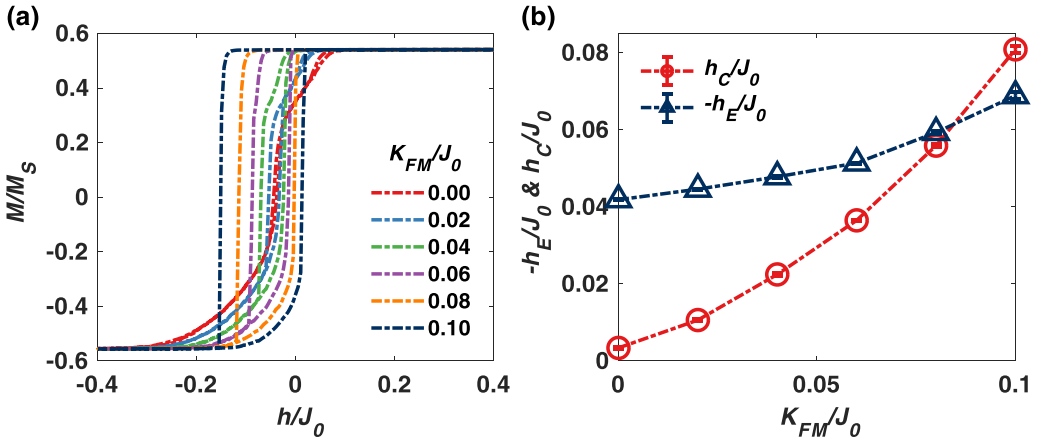

FIG. 2. (a) The hysteresis loops calculated with constrained MC and (b) the extracted h_E, h_C in core-shell structures with $0 \leqslant K_{\mathrm{FM}}/J_0 \leqslant 0.1$ after FC. All the data in (b) are averaged with three independent calculations with error bars coming from the calculated standard deviations.

AFM spins in the constrained MC. Meanwhile, both h_C and h_E given in Fig. 2(b) are larger than those obtained with nonconstrained MC, indicating stronger pinning effect of the constrained AFM magnetic moments. Further, it is worth noting that the K_{FM} dependence of h_E and h_C shows similar behavior with those obtained from nonconstrained MC calculation with monotonic dependence with K_{FM}. An increment of 64.6% in h_E is obtained in the hysteresis loop with $K_{\mathrm{FM}}/J_0 = 0.1$ compared to that with $K_{\mathrm{FM}}/J_0 = 0$, which is even a little larger than the result 51.4% obtained in nonconstrained MC.

Since the AFM spins are fixed in the constrained MC, it is demonstrated that the monotonic increase of h_E and the nonlinear increase of h_C with the increasing K_{FM} is contributed by the FM core. This can be corroborated by direct inspection of the spin configurations along the loops, as presented in the main panel of Fig. 3 for $K_{\mathrm{FM}}/J_0 = 0$. As it is evidenced by the sequence of snapshots, the reversal proceeds by quasiuniform rotation along both descending and ascending branches at magnetic fields around left and right coercive fields, respectively. The hysteresis loop shows different approaching behaviors to the two saturation directions, although both are reversible. The progressive approach to negative saturation has been proven to originate from a planar domain wall formed parallel to the FM/AFM interface [56,57]. As shown in Figs. 3(c) and 3(d), this domain wall is also observed with a spherical shape in the core-shell nanoparticle where the spins close to the core center reverse before those close to the core-shell interface in the descending branch [Fig. 3(c)], while in the approach to positive saturation [Figs. 3(a) and 3(f)], all the spins in the core rotate coherently without formation of the domain wall.

For comparison, spin configurations of the nanoparticles with FM anisotropic constant of $K_{\mathrm{FM}}/J_0 = 0.1$ are inspected. As shown in Fig. 4, the magnetization reversal along the descending branch proceeds first with quasiuniform rotation and then with a fast propagation of planar domain wall nucleated at one point of the interface, while the nucleation

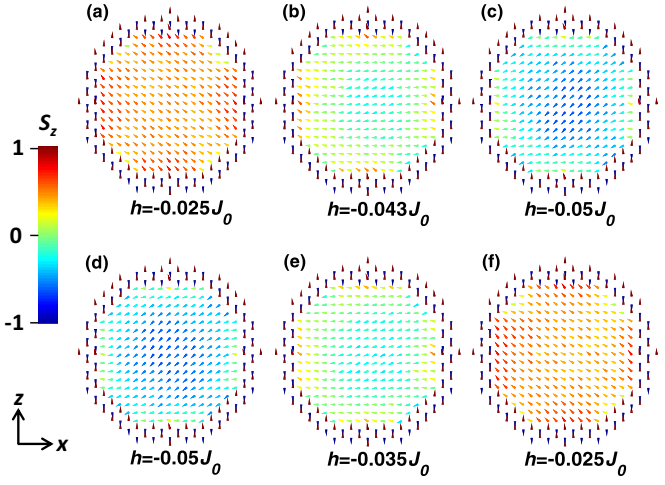

FIG. 3. Snapshots of spin configurations during magnetization reversals around the left coercive field [(a)–(c)] and right coercive field [(d)–(f)] in the system with $J_{\mathrm{FM}}/J_0 = 1$ and $K_{\mathrm{FM}}/J_0 = 0$, calculated with constrained MC. The color of the arrow indicates the magnitude of the z component of each spin.

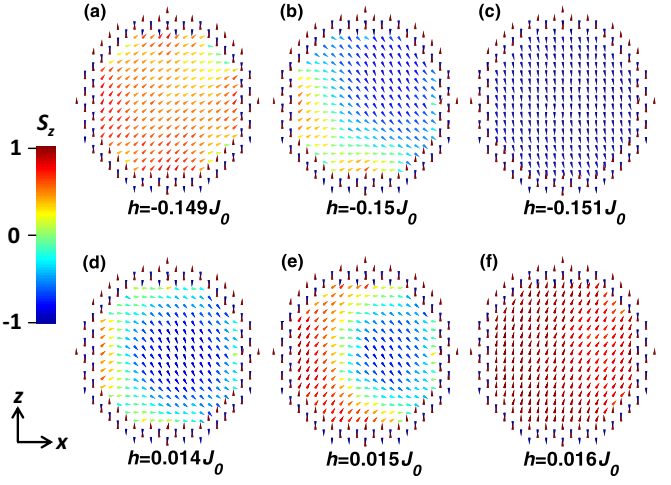

FIG. 4. Snapshots of spin configurations during magnetization reversals around the left coercive field [(a)–(c)] and right coercive field [(d)–(f)] in the system with $J_{\mathrm{FM}}/J_0 = 1$ and $K_{\mathrm{FM}}/J_0 = 0.1$, calculated with constrained MC. The color of the arrow indicates the magnitude of the z component of each spin.

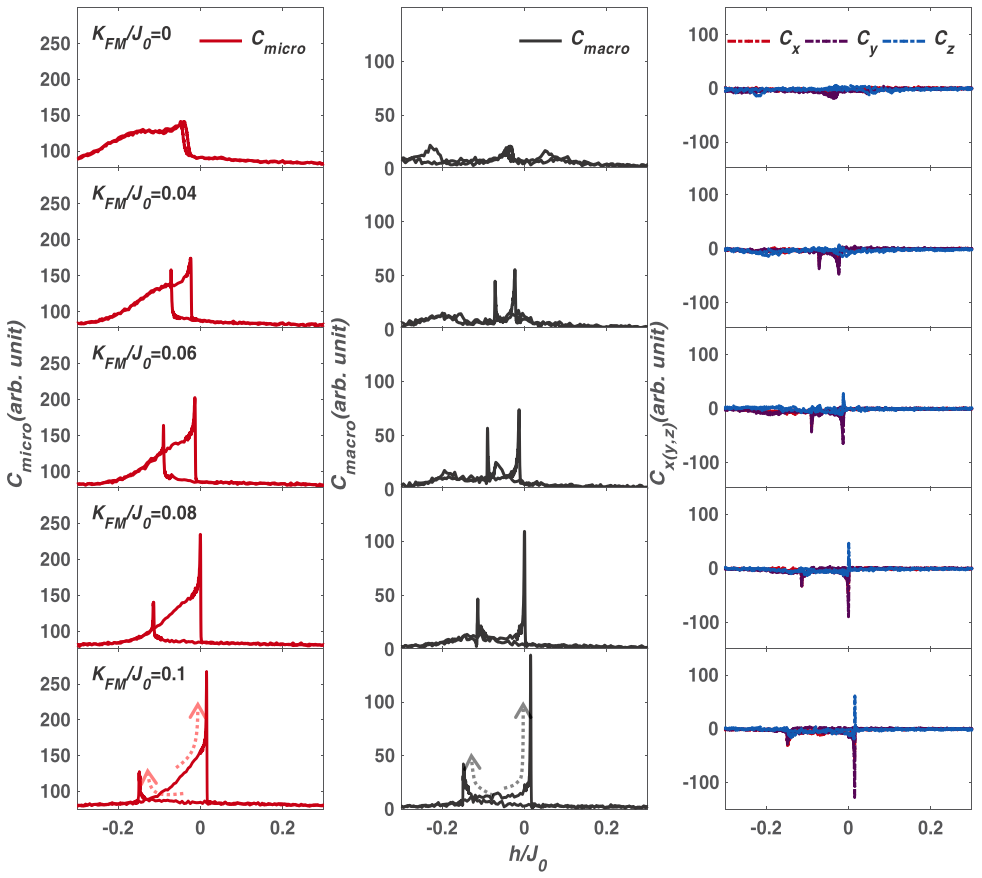

FIG. 5. The overall microscopic curls (left column), the macroscopic curls (middle column), and three different components of macroscopic curls (right column) of systems with $J_{\rm FM}/J_0 = 1$ and $0 \leqslant K_{\rm FM}/J_0 \leqslant 0.1$.

of reversed domains at the whole interface and its subsequent slow shrink across the core center is the major reversal process along the ascending branch, resulting in an asymmetric characteristic in the hysteresis loop. Similar asymmetry in hysteresis loops also has been observed experimentally in discontinuous nanostructures [2,41]. The asymmetric magnetization reversals here have similar features but different mechanisms from those obtained in continuous films, where the domain wall motion occurs in the descending branch while domain rotation occurs in the ascending branch [58,59], originating from a biaxial magnetic anisotropy in the AFM part [60].

Here, it is demonstrated that the exchange bias field is strongly correlated with a special reversal mechanism in the core-shell nanoparticle. First, $\vec{R}$, the curl of the spin vector field $\vec{S}(S_x, S_y, S_z)$ is used to describe the noncollinearity of spin configuration in the FM core, which reads

$$\begin{aligned}\vec{R} &= \nabla \times \vec{S} = R_x\vec{i} + R_y\vec{j} + R_z\vec{k} \\ &= \left(\frac{\partial S_z}{\partial y} - \frac{\partial S_y}{\partial z}\right)\vec{i} + \left(\frac{\partial S_x}{\partial z} - \frac{\partial S_z}{\partial x}\right)\vec{j} + \left(\frac{\partial S_y}{\partial x} - \frac{\partial S_x}{\partial y}\right)\vec{k}\end{aligned} \tag{4}$$

with R_x, R_y, and R_z representing three components of local curls. The differentials are calculated with a finite difference method. The vortexlike local spin configurations will yield nonzero local curls while the collinear spin configurations will give zero local curls. The overall magnitude of the microscopic (local) curls can be given as

$$C_{\rm micro} = \sum_{i\in {\rm FM}} \sqrt{R_{ix}^2 + R_{iy}^2 + R_{iz}^2}, \tag{5}$$

which enable us to get an insight into the noncollinearity of FM core, while the magnitude of macroscopic (global) curls can be represented as

$$\begin{aligned}C_{\rm macro} &= \sqrt{\left(\sum_{i\in {\rm FM}} R_{ix}\right)^2 + \left(\sum_{i\in {\rm FM}} R_{iy}\right)^2 + \left(\sum_{i\in {\rm FM}} R_{iz}\right)^2} \\ &= \sqrt{C_x^2 + C_y^2 + C_z^2},\end{aligned} \tag{6}$$

which enables us to investigate the evolution of macroscopic curling while the orientation of macroscopic curling can be obtained with its components C_x, C_y, and C_z.

As shown in Fig. 5, within a core with $K_{\rm FM}/J_0 = 0$, both overall microscopic curling $C_{\rm micro}$ and macroscopic curling $C_{\rm macro}$ show very small deviations at all fields from saturation states, which confirms that the magnetization reversals in the core are nearly coherent in both branches. However, it is worth noting that there is a significant shoulder at the left side of each coercive field in $C_{\rm micro}$, which is absent in $C_{\rm macro}$, while both $C_{\rm micro}$ and $C_{\rm macro}$ show two peaks at coercive fields.

From the spin configurations given in Figs. 3(c) and 3(d), the shoulders in C_{micro} are related to the formation of spherical domain walls in these field regions. In the spherical domain wall, the local curl at one point is opposite to that at its symmetric point, giving zero contribution to the macroscopic curl. Thus, in macroscopic curls, two peaks without shoulders around coercive fields are obtained, which are also present in microscopic curls. As K_{FM}/J_0 increases, the right peak shows a monotonic increase, while the left peak nearly does not change. From Figs. 4(b) and 4(f), it can be inferred that peaks at the left coercive fields and the right coercive fields are related to a planar domain wall and an incomplete spherical domain wall, respectively. The peak shoulder in C_{micro}, which is related to a complete spherical domain wall, is maintained in ascending branches but decreases in descending branches and finally disappears in the system with $K_{\text{FM}}/J_0 = 0.1$, showing asymmetric magnetization reversal in the two branches. Three components of macroscopic curls show similar dependence to K_{FM}/J_0. C_x and C_y always follow each other due to the rotation symmetry of the considered systems in the x-y plane. With increasing K_{FM}/J_0, both C_x and C_y peaks increase monotonically in descending branches but keep nearly invariant in ascending branches. Differently, C_z only occurs in ascending branches in systems with $K_{\text{FM}}/J_0 > 0.06$, indicating the emergence of a curling in the x-y plane.

B. Effect of exchange strength J_{FM}

The anomalous dependence of h_E and h_C on K_{FM} may originate from this asymmetric magnetization reversal behavior, which is related to different domain structures formed in descending and ascending branches. The formation of a spherical domain wall in the ascending branch of the hysteresis loop can effectively reduce the increment of right coercive field caused by increasing K_{FM} and consequently increases h_E (as shown in Fig. 2). For a classic approximation, the domain wall width of a ferromagnetic material is determined by the competition between exchange and effective anisotropic energy, which is given by

$$\delta_w = \pi\sqrt{\frac{A}{K}} = \pi\sqrt{\frac{J_{\text{FM}}}{K_{\text{FM}}}}, \tag{7}$$

where $A = nS^2 J_{\text{FM}}/a = J_{\text{FM}}$ (with $n = 1$ for simple cubic structure, $S = 1, a = 1$ for considered systems) is the exchange stiffness constant and $K = K_{\text{FM}}$ is the anisotropy constant of the material.

The K_{FM} and J_{FM} dependencies of δ_w are plotted in Fig. 6. For a given J_{FM}, δ_w decreases sharply at the beginning and then gradually in the end with the increasing K_{FM}. For a given K_{FM}, a smaller δ_w is obtained with a smaller J_{FM} than that obtained with a large J_{FM}. Consequently, given a smaller J_{FM} and a larger K_{FM}, the δ_w will be small enough to enable domain wall formation in the FM core with a diameter of $18a$. Also, the domain wall in the FM core will be suppressed with larger J_{FM} and smaller K_{FM}.

To verify this hypothesis, the K_{FM} dependence of exchange bias in this system with varying J_{FM} is studied. In all the calculations, AFM spins are constrained. As shown in Fig. 7(a), the exchange bias field h_E shows a very sharp increase with

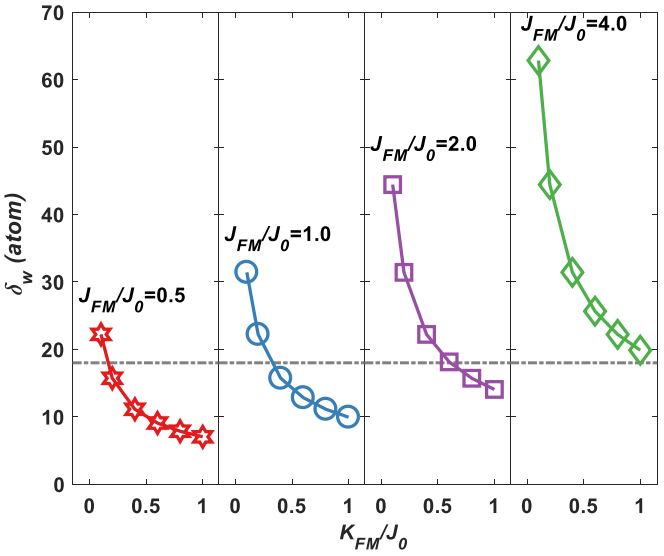

FIG. 6. The dependence of domain wall width on K_{FM} and J_{FM} calculated from Eq. (7) with a grey dashed line indicating the diameter of the FM core.

increasing K_{FM} with a small ferromagnetic exchange coupling $J_{\text{FM}}/J_0 = 0.5$. This monotonic dependence of h_E on K_{FM} remains with increasing J_{FM} up to $J_{\text{FM}}/J_0 = 2$ and finally disappears in the system with $J_{\text{FM}}/J_0 = 4$, where h_E shows no obvious dependence on K_{FM}. The effect of J_{FM} is more prominent in the relative increment of exchange bias field, $\delta h_E/h_{E0}$, where h_{E0} and δh_E are the h_E at $K_{\text{FM}}/J_0 = 0$ and the increment of h_E relative to h_{E0} at $K_{\text{FM}}/J_0 \neq 0$. As shown in Fig. 7(c), $\delta h_E/h_{E0}$ shows a very sharp increase with increasing K_{FM} in a system with $J_{\text{FM}}/J_0 = 0.5$. The increase is largely reduced in systems with larger J_{FM}. Finally, a nearly zero increment in h_E is obtained with increasing K_{FM} in the system with $J_{\text{FM}}/J_0 = 4$.

Meanwhile, h_C also shows a strong dependence on both K_{FM} and J_{FM}. As shown in Fig. 7(b), with a small J_{FM}, the system shows a superparamagnetic characteristic with nearly zero h_{C0} (the h_C at $K_{\text{FM}}/J_0 = 0$). As the J_{FM} increases, h_{C0} shows a monotonic increase, indicating an increasing magnetic anisotropy given by the exchange coupling at the core-shell interface. Consequently, the relative increment of coercivity, $\delta h_C/h_{C0}$, where δh_C is the increment of h_C relative to h_{C0} at $K_{\text{FM}}/J_0 \neq 0$, increases with K_{FM} but decreases with J_{FM}, as shown in Fig. 7(d). Moreover, it is found that the way in which h_C depends on K_{FM} varies with J_{FM} significantly. When J_{FM} is small, h_C shows a nonlinear dependence on increasing K_{FM}, with a gradual increase at lower K_{FM} and a steeper increase at higher K_{FM}. However, when J_{FM} increases, the nonlinearity of the dependence is reduced and, finally, becomes a linear dependence in the system with $J_{\text{FM}}/J_0 = 4$.

An invariant h_E and a linear dependent h_C on K_{FM} is predicted by the M-B single spin model, which is absent in a system with a small J_{FM} and is present in a system with a large J_{FM}, indicating an evolution of the spin configuration from noncollinear to collinear during magnetization reversals as J_{FM} increases, which is verified by an inspection of spin configurations and overall microscopic curls of the systems with different J_{FM} during magnetization reversals.

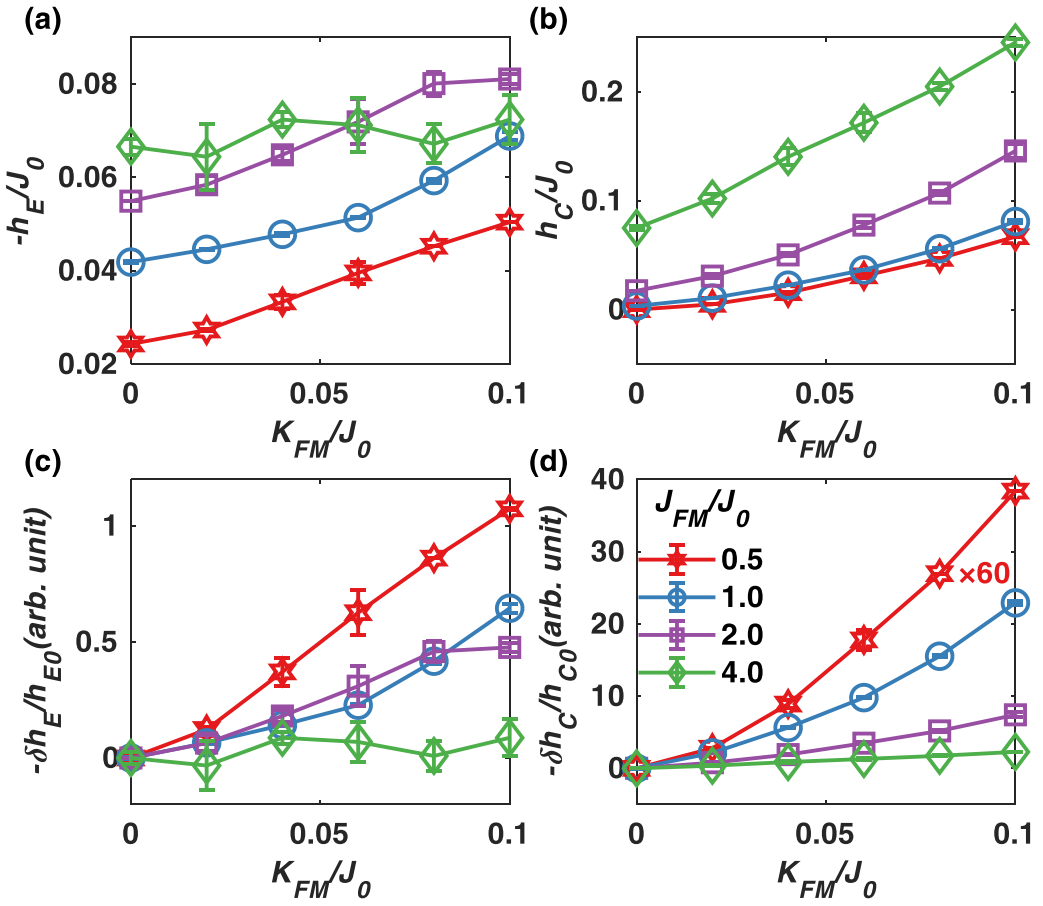

FIG. 7. The K_{FM} dependence of (a) h_E, (b) h_C, and (c) relative change of h_E and (d) relative change of h_C plots with different J_{FM}. All the data are averaged with three independent calculations with error bars coming from the calculated standard deviations.

It can be seen from the first column of Fig. 8 that the planar domain wall at the left coercive field shows strong dependence with increasing J_{FM}. The planar domain wall with a small width is very significant in a system with small J_{FM}, and becomes weaker with a larger domain wall width as J_{FM} increases. A collinear alignment of core spins and decreased contrast in color map of S_z are observed in the system with $J_{\mathrm{FM}}/J_0 = 4.0$, as shown in Fig. 8(j). The spherical domain wall at the right coercive field shows similar J_{FM} dependence as the planar domain wall, as shown in the middle column of Fig. 8, which becomes weaker and broader with increasing J_{FM} and nearly disappears in the system with $J_{\mathrm{FM}}/J_0 = 4.0$. The evolution of domain structure with J_{FM} is also reflected in the overall microscopic curls (Fig. 8, right column). As shown in Fig. 8(c), the overall microscopic curls in the system with $J_{\mathrm{FM}}/J_0 = 0.5$ are very large with contributions including a large background coming from the random thermal fluctuation, two peaks from the planar domain wall and the incomplete spherical domain wall at the left and right coercive fields, respectively, and broad shoulders from the complete spherical domain walls. With an increased J_{FM}/J_0, as shown in Figs. 8(f) and 8(i), overall, the microscopic curls are lowered significantly, which is in good agreement with the spin configurations. Meanwhile, the background is also reduced largely, which is ascribed to the effectively suppressed thermal fluctuations by the large exchange coupling. Finally, as shown in Fig. 8(l), with the largest J_{FM}/J_0 of 4.0, both the peaks and the background are largely reduced corresponding to nearly collinear spin configurations during the magnetization reversals.

For a realistic material consideration, typical domain wall widths of Fe, Co, and Ni nanoparticles are around 138, 36, and 285 nm, respectively [61]. However, the magnetic vortex state has been observed in Fe nanoparticles with a size of 26 nm [43], indicating the noncollinear magnetic configuration can be obtained in magnetic nanoparticles much smaller than the bulk domain wall width. In harder magnetic materials, a much smaller domain wall width can be obtained. For instance, domain wall widths for $CoFe_2O_4$ and $Nd_2Fe_{14}B$ are about 8 nm [62] and 5 nm [63], respectively. An incomplete spherical domain wall can exist in a nanoparticle around this length scale, which can be easily manipulated with size control and composition tailoring to give an optimized exchange bias effect and other magnetic properties.

IV. CONCLUSIONS

To conclude, the effect of FM spin configuration on the exchange bias effect of FM/AFM core-shell nanoparticles has been studied with MC method. A significant enhancement of the exchange bias effect accompanied by a nonlinear behavior of coercivity with increasing magnetic anisotropy constant K_{FM} has been observed, showing a violation of classic M-B model. This anomalous effect is ascribed to the asymmetric

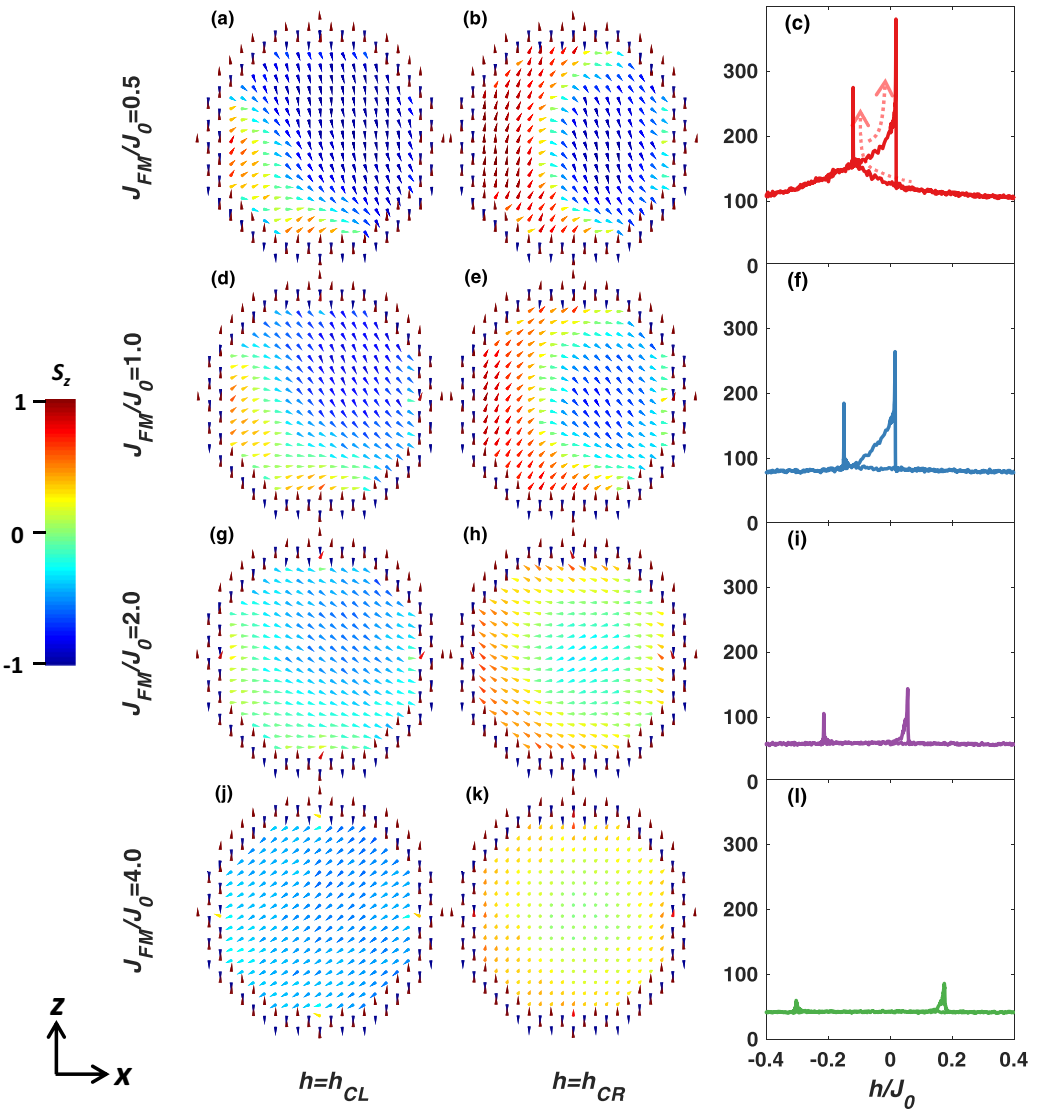

FIG. 8. Spin configuration snapshots of systems with the same $K_{\mathrm{FM}}/J_0 = 0.1$ but with $0.5 \leqslant J_{\mathrm{FM}}/J_0 \leqslant 4.0$ taken at left coercive fields (left column) and right coercive fields (middle column) and overall microscopic curls as functions of the magnetic field in systems with different J_{FM}, calculated with constrained MC. The color of the arrows in the spin configuration snapshots indicates the magnitude of the z component of each spin.

magnetization reversal in the FM core with a spherical domain wall formation in the ascending branch of the hysteresis loop, which largely reduces the right coercive field and enhances the exchange bias field. This is demonstrated by adjusting the domain wall width in the FM core with varying J_{FM} and K_{FM}. Finally, the anomalous dependence of h_E and h_C on K_{FM} disappears when the domain wall in the core is suppressed. The results provide another freedom to tailor the exchange bias in the FM/AFM systems.

ACKNOWLEDGMENTS

This work is supported by the National Key Research and Development Program of China (Grant No. 2017YFA-0206303, 2016YFB0700901 and No. 2017YFA0401502), National Natural Science Foundation of China (Grant No. 51731001, No. 51371009, No. 11504348, No. 11675006), the Ph.D. Programs Foundation of Ministry of Education of China (No. 20130001110002).

[1] W. H. Meiklejohn and C. P. Bean, Phys. Rev. **102**, 1413 (1956).
[2] K. Liu, S. M. Baker, M. Tuominen, T. P. Russell, and I. K. Schuller, Phys. Rev. B **63**, 060403 (2001).
[3] W. Zhang, A. Chen, J. Jian, Y. Zhu, L. Chen, P. Lu, Q. Jia, J. L. MacManus-Driscoll, X. Zhang, and H. Wang, Nanoscale **7**, 13808 (2015).
[4] S. Brück, G. Schütz, E. Goering, X. Ji, and K. M. Krishnan, Phys. Rev. Lett. **101**, 126402 (2008).
[5] D. Niebieskikwiat and M. B. Salamon, Phys. Rev. B **72**, 174422 (2005).
[6] M. Ali, P. Adie, C. H. Marrows, D. Greig, B. J. Hickey, and R. L. Stamps, Nat. Mater. **6**, 70 (2007).

[7] B. M. Wang, Y. Liu, P. Ren, B. Xia, K. B. Ruan, J. B. Yi, J. Ding, X. G. Li, and L. Wang, Phys. Rev. Lett. **106**, 077203 (2011).

[8] Y. H. Xia, R. Wu, Y. F. Zhang, S. Q. Liu, H. L. Du, J. Z. Han, C. S. Wang, X. P. Chen, L. Xie, Y. C. Yang, and J. B. Yang, Phys. Rev. B **96**, 064440 (2017).

[9] Y. Sun, J. Z. Cong, Y. S. Chai, L. Q. Yan, Y. L. Zhao, S. G. Wang, W. Ning, and Y. H. Zhang, Appl. Phys. Lett. **102**, 172406 (2013).

[10] A. K. Nayak, M. Nicklas, S. Chadov, P. Khuntia, C. Shekhar, A. Kalache, M. Baenitz, Y. Skourski, V. K. Guduru, A. Puri, U. Zeitler, J. M. D. Coey, and C. Felser, Nat. Mater. **14**, 679 (2015).

[11] G. Margaris, K. N. Trohidou, and J. Nogués, Adv. Mater. **24**, 4331 (2012).

[12] V. Skumryev, S. Stoyanov, Y. Zhang, G. Hadjipanayis, D. Givord, and J. Nogués, Nature (London) **423**, 850 (2003).

[13] V. F. Puntes, K. M. Krishnan, and A. P. Alivisatos, Science **291**, 2115 (2001).

[14] S. H. Sun, C. B. Murray, D. Weller, L. Folks, and A. Moser, Science **287**, 1989 (2000).

[15] D. V. Talapin, E. V. Shevchenko, M. I. Bodnarchuk, X. Ye, J. Chen, and C. B. Murray, Nature (London) **461**, 964 (2009).

[16] T. J. Yoon, H. Shao, R. Weissleder, and H. Lee, Part. Part. Syst. Charact. **30**, 667 (2013).

[17] Q. K. Ong, A. Wei, and X. M. Lin, Phys. Rev. B **80**, 134418 (2009).

[18] G. Salazar-Alvarez, J. Sort, S. Surinach, M. D. Baró, and J. Nogués, J. Amer. Chem. Soc. **129**, 9102 (2007).

[19] B. P. Pichon, O. Gerber, C. Lefevre, I. Florea, S. Fleutot, W. Baaziz, M. Ohlmann, C. Ulhaq, O. Ersen, V. Pierron-Bohnes, P. Panissod, M. Drillon, and S. Begin-Colin, Chem. Mater. **23**, 2886 (2011).

[20] A. Saha and R. Viswanatha, ACS Nano **11**, 3347 (2017).

[21] M. Estrader, A. López-Ortega, S. Estradé, I. V. Golosovsky, G. Salazar-Alvarez, M. Vasilakaki, K. N. Trohidou, M. Varela, D. C. Stanley, M. Sinko, M. J. Pechan, D. J. Keavney, F. Peiró, S. Suriñach, M. D. Baró, and J. Nogués, Nat. Commun. **4**, 2960 (2013).

[22] K. E. Marusak, A. C. Johnston-Peck, W. C. Wu, B. D. Anderson, and J. B. Tracy, Chem. Mater. **29**, 2739 (2017).

[23] M. Sytnyk, R. Kirchschlager, M. I. Bodnarchuk, D. Primetzhofer, D. Kriegner, H. Enser, J. Stangl, P. Bauer, M. Voith, A. W. Hassel, F. Krumeich, F. Ludwig, A. Meingast, G. Kothleitner, M. V. Kovalenko, and W. Heiss, Nano Lett. **13**, 586 (2013).

[24] M. Vasilakaki, K. N. Trohidou, and J. Nogués, Sci. Rep. **5**, 9609 (2015).

[25] X. L. Sun, N. F. Huls, A. Sigdel, and S. H. Sun, Nano Lett. **12**, 246 (2012).

[26] M. H. Wu, Q. C. Li, and J. M. Liu, J. Phys.: Condens. Matter, **19**, 186202 (2007).

[27] E. Wetterskog, C. W. Tai, J. Grins, L. Bergström, and G. Salazar-Alvarez, ACS Nano **7**, 7132 (2013).

[28] V. Dimitriadis, D. Kechrakos, O. Chubykalo-Fesenko, and V. Tsiantos, Phys. Rev. B **92**, 064420 (2015).

[29] K. Simeonidis, C. Martinez-Boubeta, Ò. Iglesias, A. Cabot, M. Angelakeris, S. Mourdikoudis, I. Tsiaoussis, A. Delimitis, C. Dendrinou-Samara, and O. Kalogirou, Phys. Rev. B **84**, 144430 (2011).

[30] Ò. Iglesias, X. Batlle, and A. Labarta, J. Phys. D: Appl. Phys. **41**, 134010 (2008).

[31] J.-Y. Ji, P.-H. Shih, T.-S. Chan, Y.-R. Ma, and S. Y. Wu, Nanoscale Res. Lett. **10**, 243 (2015).

[32] F. C. M. Filho, L. L. Oliveira, S. S. Pedrosa, G. O. G. Rebouças, A. S. Carriço, and A. L. Dantas, Phys. Rev. B **92**, 064422 (2015).

[33] C. Martinez-Boubeta, K. Simeonidis, A. Makridis, M. Angelakeris, Ò. Iglesias, P. Guardia, A. Cabot, L. Yedra, S. Estradé, F. Peiró, Z. Saghi, P. A. Midgley, I. Conde-Leborán, D. Serantes, and D. Baldomir, Sci. Rep. **3**, 1652 (2013).

[34] R. F. L. Evans, D. Bate, R. W. Chantrell, R. Yanes, and O. Chubykalo-Fesenko, Phys. Rev. B **84**, 092404 (2011).

[35] J. A. González, J. P. Andrés, R. L. Antón, J. A. D. Toro, P. S. Normile, P. Munñiz, J. M. Riveiro, and J. Nogués, Chem. Mater. **29**, 5200 (2017).

[36] W. H. Meiklejohn and C. P. Bean, Phys. Rev. **105**, 904 (1957).

[37] J. Nogués and I. K. Schuller, J. Magn. Magn. Mater. **192**, 203 (1999).

[38] R. Morales, A. C. Basaran, J. E. Villegas, D. Navas, N. Soriano, B. Mora, C. Redondo, X. Batlle, and I. K. Schuller, Phys. Rev. Lett. **114**, 097202 (2015).

[39] F. Radu, M. Etzkorn, R. Siebrecht, T. Schmitte, K. Westerholt, and H. Zabel, Phys. Rev. B **67**, 134409 (2003).

[40] J. F. Löffler, H.-B. Braun, and W. Wagner, Phys. Rev. Lett. **85**, 1990 (2000).

[41] Y. Ijiri, C. V. Kelly, J. A. Borchers, J. J. Rhyne, D. F. Farrell, and S. A. Majetich, Appl. Phys. Lett. **86**, 243102 (2005).

[42] E. Pinilla-Cienfuegos, S. Manñas-Valero, A. Forment-Aliaga, and E. Coronado, ACS Nano. **10**, 1764 (2016).

[43] C. Gatel, F. J. Bonilla, A. Meffre, E. Snoeck, B. Warot-Fonrose, B. Chaudret, L. M. Lacroix, and T. Blon, Nano Lett. **15**, 6952 (2015).

[44] Ò. Iglesias, X. Batlle, and A. Labarta, Phys. Rev. B **72**, 212401 (2005).

[45] L. B. Ho, T. N. Lan, and T. H. Hai, Physica B **430**, 10 (2013).

[46] Y. Hu, Y. Liu, A. Du, and F. Shi, Phys. Lett. A **378**, 1667 (2014).

[47] Y. Yüksel and Ü. Akıncı, J. Phys.: Condens. Matter **28**, 486003 (2016).

[48] Ò. Iglesias and A. Labarta, Physica B **343**, 286 (2004).

[49] N. Metropolis, A. W. Rosenbluth, M. N. Rosenbluth, A. H. Teller, and E. Teller, J. Chem. Phys. **21**, 1087 (1953).

[50] D. Hinzke and U. Nowak, Comput. Phys. Commun. **121–122**, 334 (1999).

[51] G. Marsaglia, Ann. Math. Stat. **43**, 645 (1972).

[52] F. Hellman, A. L. Shapiro, E. N. Abarra, R. A. Robinson, R. P. Hjelm, P. A. Seeger, J. J. Rhyne, and J. I. Suzuki, Phys. Rev. B **59**, 11408 (1999).

[53] L. L. Hinchey and D. L. Mills, Phys. Rev. B **34**, 1689 (1986).

[54] N. C. Koon, Phys. Rev. Lett. **78**, 4865 (1997).

[55] T. C. Schulthess and W. H. Butler, Phys. Rev. Lett. **81**, 4516 (1998).

[56] Z.-P. Li, O. Petracic, R. Morales, J. Olamit, X. Batlle, K. Liu, and I. K. Schuller, Phys. Rev. Lett. **96**, 217205 (2006).

[57] J. Mejia-Lopez, R. Ramirez, and M. Kiwi, J. Magn. Magn. Mater. **241**, 364 (2002).

[58] W. -T. Lee, S. G. E. te Velthuis, G. P. Felcher, F. Klose, T. Gredig, and E. D. Dahlberg, Phys. Rev. B **65**, 224417 (2002).
[59] S. Brems, D. Buntinx, K. Temst, C. Van Haesendonck, F. Radu, and H. Zabel, Phys. Rev. Lett. **95**, 157202 (2005).
[60] A. Hoffmann, Phys. Rev. Lett. **93**, 097203 (2004).
[61] D. C. Jiles, *Introduction to Magnetism and Magnetic Materials* (CRC Press, London, 1998).
[62] Q. Song and Z. J. Zhang, J. Am. Chem. Soc. **134**, 10182 (2012).
[63] S. J. Lloyd, J. C. Loudon, and P. A. Midgley, J. Microsc. **207**, 118 (2002).